APL Materials

Effects of microstructure and growth conditions on quantum emitters in gallium nitride

Minh Nguyen, Tongtong Zhu (iD), Mehran Kianinia, Fabien Massabuau (iD), Igor Aharonovich (iD), Milos Toth, Rachel Oliver (iD), and Carlo Bradac (iD)

View Online   Export Citation   CrossMark

ARTICLES YOU MAY BE INTERESTED IN

ORDER PRINT EDITION

AIP Conference Proceedings
The 18th International Conference on Positron Annihilation

Effects of microstructure and growth conditions on quantum emitters in gallium nitride

View Online   Export Citation   CrossMark

Minh Nguyen,[1,a] Tongtong Zhu,[2,a] (iD) Mehran Kianinia,[1] Fabien Massabuau,[2] (iD) Igor Aharonovich,[1] (iD)
Milos Toth,[1] Rachel Oliver,[2,b] (iD) and Carlo Bradac[1,b] (iD)

AFFILIATIONS

[1] School of Mathematical and Physical Sciences, University of Technology Sydney, Ultimo, New South Wales 2007, Australia
[2] Department of Materials Science and Metallurgy, University of Cambridge, Cambridge CB3 0FS, United Kingdom

[a] Contributions: M. Nguyen and T. Zhu contributed equally to this work.
[b] Authors to whom correspondence should be addressed: rao28@cam.ac.uk and carlo.bradac@uts.edu.au

ABSTRACT

Single-photon emitters in gallium nitride (GaN) are gaining interest as attractive quantum systems due to the well-established techniques for growth and nanofabrication of the host material, as well as its remarkable chemical stability and optoelectronic properties. We investigate the nature of such single-photon emitters in GaN with a systematic analysis of various samples produced under different growth conditions. We explore the effect that intrinsic structural defects (dislocations and stacking faults), doping, and crystal orientation in GaN have on the formation of quantum emitters. We investigate the relationship between the position of the emitters—determined via spectroscopy and photoluminescence measurements—and the location of threading dislocations—characterized both via atomic force microscopy and cathodoluminescence. We find that quantum emitters do not correlate with stacking faults or dislocations; instead, they are more likely to originate from point defects or impurities whose density is modulated by the local extended defect density.

INTRODUCTION

Nonclassical single photon emitters (SPEs) are one of the most fundamental components of quantum-based technologies—quantum computation,[1–3] quantum simulation,[4] quantum metrology,[5] and quantum communication.[6] In particular, SPEs based on atomlike emitters in solid-state systems are widely studied. They combine the outstanding optical properties of atoms with the convenience and scalability of a solid-state host, hence constituting an ideal candidate for the practical realization of quantum-based devices. Some of the most prominent solid-state, room-temperature SPEs include color centers in diamond,[7–9] silicon carbide,[10,11] zinc oxide,[12,13] and hexagonal boron nitride.[14,15] In this context, single-photon emitters in gallium nitride (GaN) are emerging as an attractive alternative. The reason is twofold. The first is fundamental: recently GaN was found to host bright quantum emitters which are optically stable at room-temperature and emit over a wide range of wavelengths, from the UV to the infrared[16,17]—yet their exact nature is still unknown. Although emitters in iC

and diamond exist, studies of quantum effects in the nitride family are important due to its technological maturity and its potential for hosting spin systems.[18–20] The second is practical: GaN is a well-known semiconductor with remarkable chemical stability and optoelectronic properties, in addition to established growth and nanofabrication techniques which have made it an ideal platform for integrated photonic, commercial light emitting diodes (LEDs), and large-volume data storage technologies.[21,22] This means that GaN offers the unique opportunity—which is the focus of this study—to explore and understand the nature of the quantum emitters located within its crystalline matrix, while potentially allowing for the design of strategies for controlling and ultimately engineering their properties. This aspect is key, as controlling the quality—e.g., the accurate positioning of the emitters, the indistinguishability of the generated photons, as well as the ability to efficiently extract them from the crystalline matrix—is one of the major challenges many of the identified solid-state SPEs are still facing due to the complexity of the mesoscopic environment of the host material.[23]

GaN synthesis can be conducted via epitaxial growth on various substrates and following different protocols.[21,24] Currently, most growth methods still involve the use of foreign substrates such as silicon, silicon carbide, or sapphire.[24] The flexibility to choose both procedures and substrate means that bulk GaN can be tailored to form distinct crystalline (hetero)structures such as a-plane and c-plane layers.[25–27] Growth of GaN on non-native substrates also means that the large lattice as well as thermal expansion mismatch between the substrate and GaN can result in the formation of extended defects [e.g., threading dislocations (TDs)] and stacking faults, with the dominant defect depending on the growth orientation.[21,28] In addition, foreign atoms can be readily introduced in the GaN matrix during synthesis.[29,30] Although GaN devices seem to be remarkably robust to extended defects compared to many other semiconductors, TDs do result in a deterioration of the optical and electronic performance observed in GaN devices[31,32]—e.g., through carrier scattering and nonradiative recombination processes. However, it is still unknown whether they play any role in the formation of quantum emitters. It has previously been hypothesized that the formation of GaN quantum emitters is associated with extended structural defects created during GaN epitaxy. To test this hypothesis and explore the nature of the quantum emitters, we perform a systematic study of a number of GaN samples differing from one another in their density of TDs, the presence or absence of stacking faults, their doping, growth orientation, and geometry. We provide a detailed optical and spatial analysis of the quantum emitters found in each sample. We then investigate in detail the spatial correlation between the emitters found by photoluminescence (PL) and the position of the TDs in the GaN lattice identified by cathodoluminescence (CL) and atomic-force microscopy (AFM).

Quantum emitters in GaN have previously been hypothesized to relate to stacking faults.[17] We find no evidence for this contention in the current study. Instead, they are more likely to be due to point defects or impurities occurring at very low concentration but with a density which is affected by the local extended defect density. This work furthers our understanding of how quantum emitters are created in GaN and provides information for the potential engineering of GaN-based scalable, integrated devices for advanced photonic and quantum applications.

RESULTS AND DISCUSSION

Sample growth and AFM characterization

We analyzed eight different GaN samples, labeled A–H, each one synthesized under specific growth conditions. The goal was to explore—and potentially tailor—the effects different parameters would have on the formation of quantum emitters in GaN. Each one of the eight samples was thus synthesized to control for a set of specific characteristics: density of dislocations (Samples A, B, and C), doping of the matrix with extrinsic impurities expected to create deep-level states [e.g., with carbon (C) and iron (Fe) atoms: Samples D and E], growth substrate (e.g., GaN grown on silicon, Sample F) and orientation of the grown GaN material itself and hence the nature of the dominant extended defect (e.g., nonpolar and semipolar: Samples G and H). Samples A–E are c-plane layers in which the dominant extended defects are TDs, samples G and H are nonpolar

and semipolar, respectively, and the dominant extended defects are basal plane stacking faults.

The samples were grown using metal-organic vapor phase epitaxy on two different substrates, sapphire and silicon.[33,34] Trimethyl gallium and ammonia were used as precursors and hydrogen as the carrier gas during the various growth processes. Figures 1(a)–1(h) show the schematic diagrams of the cross section for each one of the different samples. Figures 1(a′)–1(h′) show the corresponding topographic features—such as the surface terminations of crystallographic defects—as characterized by AFM. The following is a summary of the rationale behind the growth of each sample; the growth parameters are described in more detail in the Methods section.

(i) Samples A, B, and C are c-plane (0001) GaN, which were deliberately grown under different conditions to have a substantial difference in the density of TDs in the GaN epitaxial layer: Sample A to have a high dislocation density of $\sim 5 \times 10^9$ cm^{-2} (HDD) and Sample B a low dislocation density of $\sim 3 \times 10^8$ cm^{-2} (LDD). An even lower density of TDs ($\sim 3 \times 10^7$ cm^{-2} in this case) can be achieved using epitaxial lateral overgrowth (ELOG), Sample C. The intent for these samples is to establish whether the number and position of crystallographic extended defects correlate with the number and position of deep defect states in the material, which has been the object of thorough, yet nondefinitive, research.[35] We note that these samples are not expected to contain any significant density of extended stacking faults, although stacking nm-scale stacking faults may occur when mixed dislocations dissociate. We base this comment on transmission electron microscopy studies of samples grown under similar conditions across a period of more than 10 years. Stacking faults are only typically seen in these c-plane materials either very occasionally in the region immediately adjacent to the GaN/sapphire interface, or when the growth is disrupted by a regrowth interface or heterostructure.[36] Neither of the latter two points is relevant to these samples.

(ii) Samples D and E were grown with the intent to study the effects of extrinsic doping during growth, i.e., whether impurities—which in wide-bandgap materials can result in the formation of deep-level states in the bandgap—would create optically active color centers within the GaN host matrix.[13,23] Samples D and E were synthesized to intentionally contain a high concentration of Carbon (C-doped) at 1.5×10^{19} cm^{-3} and Iron impurities (Fe-doped) at 1×10^{18} cm^{-3}, respectively.

(iii) Sample F was synthesized to investigate the formation of emitters in relation to the substrate on which the GaN structure was grown on. In this respect, GaN is a favorable choice as the wide availability of different methods of GaN growth allows for its synthesis on a variety of different substrates. Specifically, Sample F consists of n-doped, c-plane GaN grown on silicon. This resulted in an estimated threading dislocation density of 2×10^9 cm^{-2}.

(iv) Samples G and H were synthesized to explore the effect of crystal orientation on the potential creation of optically active defects. Sample G is nonpolar (11-20) GaN, while
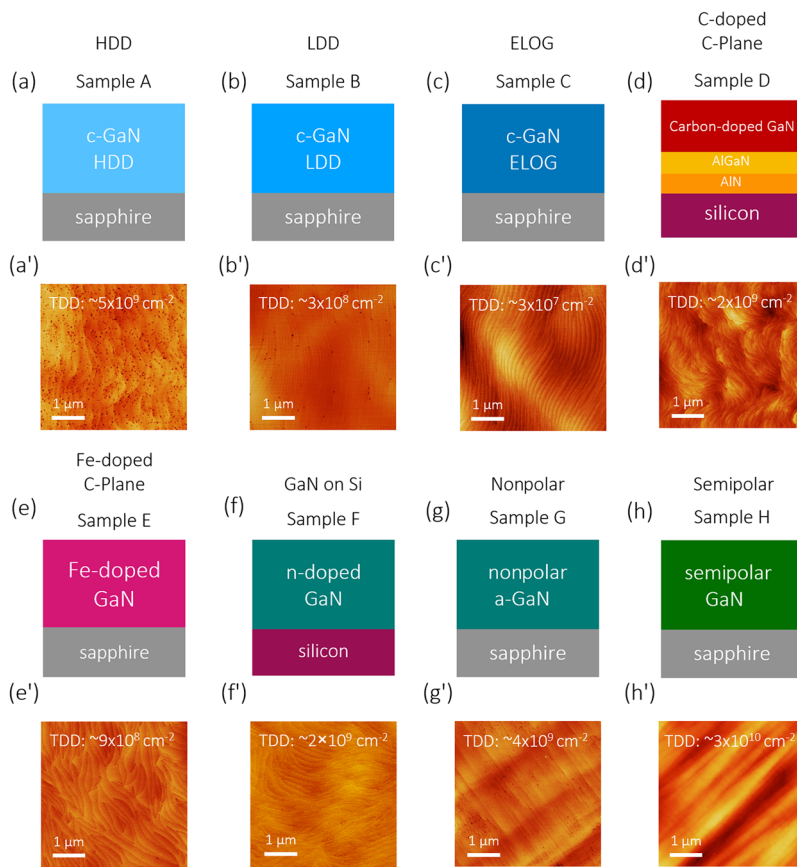
FIG. 1. Schematic and topographical characterization of all GaN samples investigated. [(a)–(h)] Schematics of c-plane HDD GaN (a), c-plane LDD GaN (b), c-plane ELOG GaN (c), C-doped GaN (d), Fe-doped GaN (e), n-doped GaN grown on silicon (f), nonpolar GaN (g), and semipolar GaN (h). [(a′)–(h′)] Topographical AFM scans for each corresponding sample. The threading dislocation density (TDD) is noted for each topographical scan.

Sample H is semipolar (11-22) GaN. Heteroepitaxial nonpolar and semipolar GaN are known to contain large densities of partial dislocations and stacking faults, but stacking faults may be considered the dominant extended defect. Sample G has an estimated TD density[37] of 3×10^{10} cm^{-2} and a basal plane stacking fault density of 3×10^5 cm^{-1}, while Sample H has an estimated TD density[38] of 4×10^9 cm^{-2} and a basal plane stacking fault density of 2×10^5 cm^{-1}. Hence, we can use these samples to probe if stacking faults are playing any role in the formation of SPEs in GaN. Moreover, the unintentional impurity incorporation rate in semipolar material is faster than in the nonpolar one so that the doping in the nonpolar and semipolar sample will also differ, with a much higher density of oxygen impurities in the semipolar sample.[39]

PL characterization

In order to probe quantum emission from SPEs in GaN at room temperature, we performed PL measurement on all the eight samples. The samples were characterized in a lab-built confocal microscope described elsewhere.[40] Briefly, the specimens were excited with a 532-nm continuous wave laser through a 0.9-NA air-objective. The emitted light was collected back through the same objective, spectrally filtered and sent either to a spectrometer or to

two avalanche photodiodes (APDs) arranged in a Hanbury Brown and Twiss (HBT) interferometer configuration for single-photon detection.

The PL spectroscopy measurements carried out on the eight samples are summarized in Fig. 2. All samples grown on sapphire substrates displayed an intense background PL emission peak at 695 nm—which is known to be due to chromium impurities in sapphire.[41] Samples A, B, E, and H showed strong PL emission at other wavelengths. Figures 2(a), 2(b), 2(e), and 2(h) show the spectra collected from each sample—the analyzed areas are displayed in the corresponding confocal scans [Figs. 2(a′), 2(b′), 2(e′), and 2(h′)]. Note that due to the high background signal, the emitters could not be clearly identified in the PL confocal scan; we thus relied on spectroscopy measurements to isolate the individual emitters. Samples A (HDD) and B (LDD) showed a high density of emitters with zero phonon line (ZPL) wavelengths ranging from 570 nm to 750 nm. Sample E (Fe-doped) showed distinct PL emission peaks at ~710 nm and ~750 nm, but the density of emitters was qualitatively lower than that observed in Samples A and B. In samples C, D, F, and G no emitters but only broad PL emission [Figs. 2(c), 2(d), 2(f), and 2(g)] was observed (note: the sharp peak in 2f is the Raman peak from the silicon substrate).

To gather more information about the origin of the PL signal from the various samples, we conducted a more detailed analysis. For the HDD Sample A, LDD Sample B, Fe-doped Sample E,
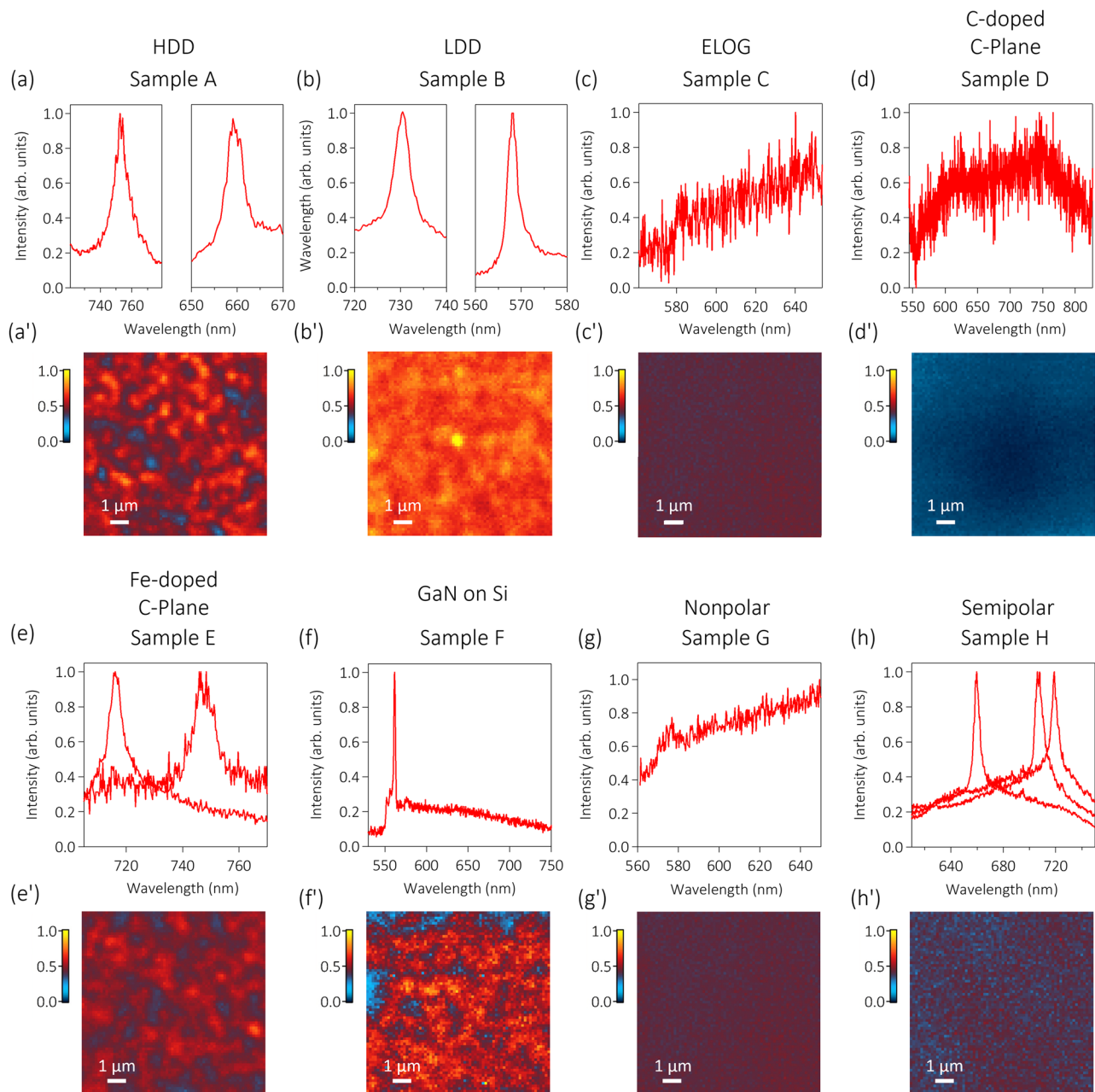
FIG. 2. PL analysis of the emitters found in the GaN samples. [(a)–(h)] Representative PL spectra of various spots taken from each sample. Sample A, B, E, and H show distinct peaks associated with the PL of single emitters, while samples C, D, F, and G display a rather broad PL signal (the sharp peak in F is the Raman peak from the silicon substrate). [(a′)–(h′)] Corresponding 10 × 10 μm^2 confocal scans where the spectroscopy measurements were conducted. Specifically: HDD GaN [(a) and (a′)], LDD GaN [(b) and (b′)], ELOG GaN [(c) and (c′)], C-doped GaN [(d) and (d′)], Fe-doped GaN [(e) and (e′)], GaN on Si [(f) and (f′)], nonpolar GaN [(g) and (g′)] and semipolar GaN [(h) and (h′)]. All spectra were acquired upon excitation via a 532-nm CW laser.

and semipolar Sample H we measured the depth along the z-axis (orthogonal to the surface) at which the emitters were located in the GaN crystal. This was achieved by collecting consecutive spectra of each emitter at multiple z-positions by varying the sample-to-objective distance in the confocal microscope. The plots from reference emitters in LDD, HDD, Fe-doped, and semipolar samples are shown in Figs. 3(a)–3(d). Interestingly, we observed that the emission in the HDD, LDD, and Fe-doped samples did not originate from emitters at the surface of the GaN crystal but rather from centers located deeper in the material, ~1–2 μm beneath the surface.
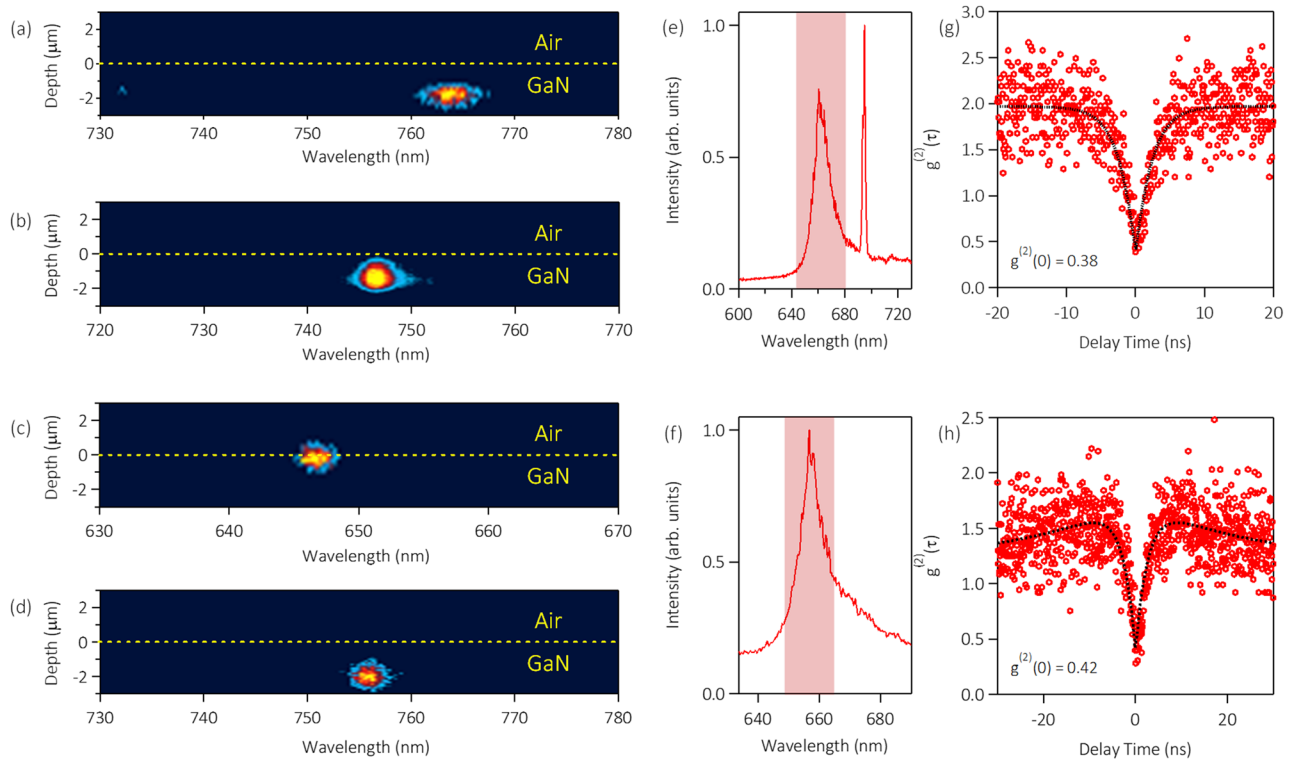
FIG. 3. Optical analysis of emitters in GaN. [(a)–(d)] Depth-resolved PL measurements of emitters in HDD (a), LDD (b), Fe-doped (c), and (d) semipolar GaN. The yellow line indicates the boundary between the GaN surface and air. All depth scans were probed with 532 nm CW excitation. [(e) and (f)] Spectrum of representative emitters in LDD GaN chosen for autocorrelation measurements. The red box indicates the bandwidth of the collected signal after filters were used to eliminate background emission. [(g) and (h)] Corresponding second order autocorrelation measurements $g^{(2)}(\tau)$ of the emitters in (e) and (f) showing their quantum nature [i.e., $g^{(2)}(0) \leq 0.5$]. Spectroscopy and autocorrelation measurements were performed with 532-nm CW excitation.

Conversely, in the semipolar sample H, the emitters were found to be mostly at the surface (see discussion below).

We also studied the photon statistics of the PL emission with a HBT interferometer to investigate the presence of single-photon sources. For the emitters in Sample A (HDD), we measured values for the second-order autocorrelation function $g^{(2)}(\tau = 0) < 1$ (not background-corrected), yet not <0.5—considered indicative of single-photon emission. This suggests that in this sample the centers are clustered in groups of at least a few emitters per confocal spot area (linear size ~500 nm). Single-photon emitters were instead found in Sample B (LDD). Figures 3(e) and 3(f) show typical PL spectra from isolated emitters in the LDD GaN sample. As stated above, the peak at 695 nm [Fig. 3(e)] originates from chromium impurities in the sapphire substrate and has been excluded in the autocorrelation measurement by applying a filter in the collection path—the spectral window analyzed is shaded in red in Figs. 3(e) and 3(f). The relevant second-order autocorrelation measurements are displayed in Figs. 3(g) and 3(h) which show values for $g^{(2)}(\tau = 0)$ of 0.38 and 0.42, respectively (values are not background-corrected)—indicative of the quantum nature of the emitters.

Whilst the HDD and LDD samples were grown under the same conditions indicating that the nature of the emitters is likely the same, it is worth noting that the two samples involved different early

stages of the growth, which results in different impurity (mainly oxygen) incorporation in the region adjacent to the GaN/sapphire interface. However, the depth of the emitters identified from the confocal PL measurements does not correspond to this near-interface region and at the relevant depth both samples have similar (low) oxygen concentrations of 3×10^{16} cm^{-3}. The two samples mainly differ in the density of TDs—these being higher in the HDD sample than in the LDD one—which seems to correlate with the corresponding density of emitters—again higher in the HDD sample than in the LDD one. To quantify this precisely, we analyzed the confocal scans (5×5 μm^2 area) of the two samples and compared directly the total number of emitters [Figs. 2(a′) and 2(b′)]. In the HDD Sample A, we identified 53 spots containing emitters vs the 17 of the LDD Sample B. These amount to values for the planar density of emitters $\geq 2.1 \times 10^8$ emitters/cm^2 and $\geq 0.7 \times 10^8$ emitters/cm^2 for samples A and B, respectively. Simultaneously, the dislocation densities estimated from the growth process for the HDD and LDD GaN samples were ~5×10^9 and ~3×10^8 dislocations/cm^2, respectively. Our analysis suggests that a higher density of TDs corresponds to a higher density of emitters, with the caveats that the overall density of emitters is significantly lower (~4–25×) than that of the TDs, and that the TDs-to-emitters correlation is nontrivial—in our analysis a ~17× increase in TDs between Sample B and A corresponds to

only a ~3× increase in emitter density. Note that for Sample A, due to the inability to identify single emitters clustered within the resolution limit of the confocal spot, the total number of emitters is underestimated—in fact, each bright spot in the confocal scan contains a few emitters, as indicated by the value of the second order autocorrelation measurement: $0.5 < g^{(2)}(0) < 1$. Undoped LDD samples typically contain about 50% edge and 50% mixed TDs (of which 50% of the mixed dislocations are undissociated and 50% are dissociated—i.e., two partial dislocations connected by a nanometer-size stacking fault). However, undoped HDD samples typically contain about 80% edge and 20% mixed dislocations (of which 50% of the mixed dislocations are undissociated and 50% are dissociated).[42] Given that we do not see a correlation between emitters and the presence of stacking faults (see below), it is unlikely that mixed-type dissociated dislocations relate to emitters. Hence, the density of emitters may correlate more closely with the density of mixed-type undissociated dislocations. We note that for the ELOG sample, which shows no emitters, the dislocation density varies periodically in bands across the surface and we might thus expect to see corresponding bands of emitters, but this effect is absent. Overall, our data lead us to posit a link between dislocations and emitters—yet not a simple one-to-one correlation. It should be highlighted here that these data provide no evidence for the previously hypothesized link between emitters and stacking faults[17] since there is no evidence for the presence of extended stacking faults in these samples and the samples with a significant stacking fault density show few or no emitters. On the other hand, we did not find any emitters in Sample F that was grown on silicon, despite a similar dislocation density to Sample B. This again suggests the relationship between the emitters and TD density is nontrivial and on a practical level suggests that sapphire may be the better substrate to use when trying to engineer emitters.

To further analyze the relationship between dislocations and emitters, we used a multimicroscopy approach (cf. Methods) to link the specific structural defects and optical signatures of those quantum emitters in GaN and carried out correlated characterization of the GaN samples via cathodoluminescence (CL) and atomic force microscopy (AFM) and combined them with the photoluminescence (PL) data. The idea was to pinpoint the potential role of TDs on the formation of luminescent quantum emitters—i.e.,

establishing whether there is a direct spatial correlation between the positions of the emitters, characterized by PL, and the position of any TDs, measured by AFM and CL. Figure 4 summarizes the result for Sample B (LDD), chosen for reference. In the figure, the same region is analyzed with the different techniques. Figure 4(a) is an AFM scan of the area: crystallographic defects terminating at the surface (blue circles) are visible as pits with a diameter of <10 nm. In this scan, mixed TDs are visible but the smaller pits related to edge TDs are not resolved. Figure 4(b) is the corresponding CL image: the dark spots arise due to nonradiative recombination at the dislocations' sites[43] and relate to both mixed and edge TDs. Hence, where the CL image black spots and AFM blue dots both show a feature in Fig. 4(c), it is likely to be a mixed dislocation, whereas when the CL image shows a feature which is not present in the AFM one, it is likely to be an edge dislocation. The density of TDs measured via CL is ~4×10^8 cm^{-2} and is consistent with the value of ~3×10^8 cm^{-2} estimated from the growth process. In Fig. 4(b), the overlaid red dots indicate the positions of the emitters measured separately in PL. Figure 4(c) is an overlay of all these measurements and highlights a few interesting aspects.

We do not find any obvious correlation between the position of the emitters detected in PL [red dots in Fig. 4(c)] and the dislocations measured by AFM and CL [blue dots and black spots in Fig. 4(c), respectively]. We can thus exclude the possibility that TDs result in discrete states in the bandgap which localize the electron-hole pair. If they did, in Fig. 4(c), every blue dot (AFM) would align with a black spot (CL) and a red dot (PL). Hence, we must consider why the TD density might correlate with the emitter density, without a direct spatial correlation between the two.

One possibility is that the subsurface TD structure is not reflected in the CL and AFM measurements; we thus used transmission electron microscopy (TEM) to investigate the structure of the TDs at the depth from which the emitters have been identified to originate in the confocal PL studies (1–2 μm below the top surface). Figure 5 shows the results of such TEM analysis for two different regions of the LDD sample, with Figs. 5(a) and 5(b) ($\boldsymbol{g} = 11\bar{2}0$) showing both edge and mixed dislocations, and Figs. 5(c) and 5(d) ($\boldsymbol{g} = 0002$) showing only mixed dislocations (note that screw-type dislocations would be visible under $\boldsymbol{g} = 0002$, if any). In all cases,
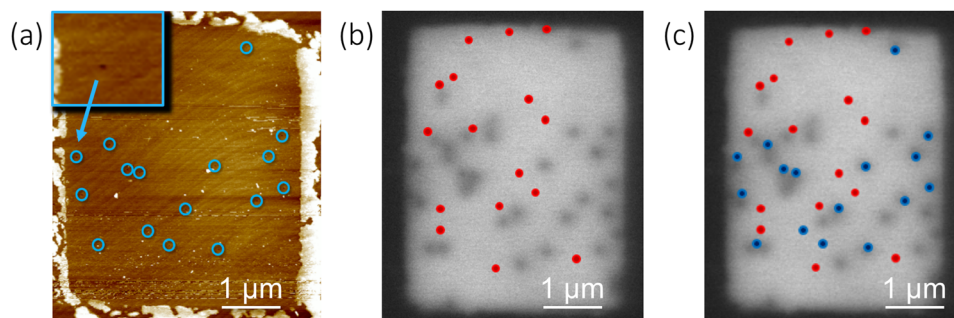

FIG. 4. AFM, panchromatic CL, and PL measurements of LDD Sample B correlating the position of threading dislocations with the optical properties of GaN emitters. (a) AFM image of the characterized grid showing the positions (blue circles) of the dislocations as they terminate at the surface. Inset shows a magnified region in the grid specifically identifying a characteristic threading dislocation as imaged by AFM. (b) CL image of the same area. The (red dots) indicate the position of single photon emitters (SPEs) as characterized separately by confocal microscopy under 532-nm CW laser excitation (confocal scan not shown). The TDs appear as (black spots) in the CL image. (c) Overlay of images (a) and (b) showing the correlation between surface features spatially characterized in AFM (blue dots) and CL (black spots), and emitters characterized in PL (red dots).
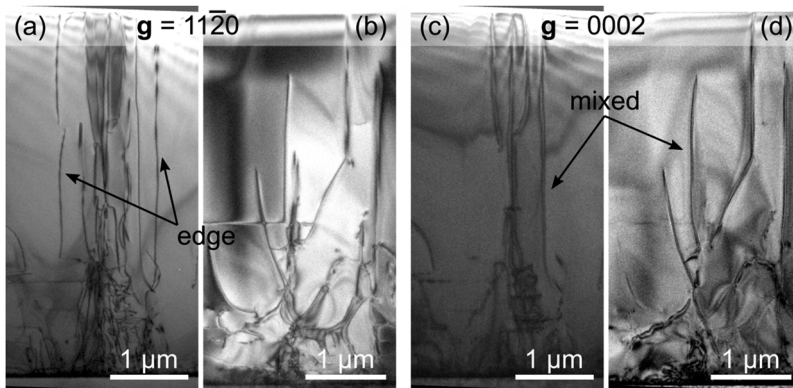
FIG. 5. TEM analysis. Cross-sectional TEM images of Sample B (LDD), observed along the $1\bar{1}00$ zone-axis and diffraction conditions $g = 11\bar{2}0$ [(a) and (b)] and $g = 0002$ [(c) and (d)]. Edge-type dislocations are visible under $g = 11\bar{2}0$ but not when $g = 0002$. Inversely, screw-type dislocations are visible under $g = 0002$ but not when $g = 11\bar{2}0$—none could be seen in this image. Mixed-type dislocations can be seen under both conditions. Note that for all images, the GaN/sapphire interface is located very close to the bottom of the image and the original GaN surface is located close to the top of the image.

the TDs run roughly vertically and are observe at a depth of 1–2 μm below the surface; very little bending is seen so that the CL and AFM images may be expected to be representative of the dislocation positions at this depth. At greater depths (3–5 μm below the surface, close to the GaN/sapphire interface) significant dislocation bending is observed, which relates to the 3D growth step used to reduce the dislocation density. However, the available data provide no evidence that these dislocations—which lie within the c-plane of GaN, and do not thread—contribute to the formation of quantum emitters.

As noted above, whilst the most obvious difference between the LDD and HDD GaN is the dislocation density, the 3D growth mode used to generate LDD GaN does result in unintentional incorporation of oxygen in the near interface region. Whilst the average thickness of this unintentionally doped layer is only about 1 μm, this unintentional doping might extend further into the film, in places. For the HDD GaN, where no 3D growth step is used, the unintentional doping throughout the film is low. For the ELOG sample, inclined facets which encourage the incorporation of unintentional dopants can persist for several microns, resulting in a layer of unintentionally n-doped material of significant thickness. Hence, samples with a higher incorporation of unintentional dopants, i.e., samples with a higher density of shallow donors, tend to have a lower density of point defects that can potentially act as quantum emitters. (The one exception to this is the semipolar sample, in which some emitters are seen despite a high density of unintentional doping. However, this sample is altogether atypical since the emitters are observed at the surface in this case—while the subsurface for all the other samples—and these emitters may thus have a distinctly different origin).

Given the lack of correlation between the actual dislocation position and the emitters, but the fact that there is a correlation between the emitters and the dislocation density, one must then consider whether extrinsic impurities or point defects might be the source of the emission and then ask how the density of such impurities away from the dislocations might be affected by the dislocation density. The following considerations hint at a potential interpretation. Local variations in dislocation density affect the strain state of the film, altering bulk and/or surface diffusion coefficients. Changes to the bulk diffusion coefficient could affect the diffusion of impurities from the sapphire into the GaN film, whilst changes to the surface or bulk diffusion coefficients may affect independently the density of nonimpurity point defects. Processes occurring at

surfaces will also be affected by changes to the surface morphology and we note that HDD GaN films are rougher, with more distorted step edges than LDD or ELOG films, potentially providing more sticking sites for impurity atoms and hence altering the incorporation rate of sparse impurities from the gas phase. (The low density of emitters indicates that such impurities must exist at such a low concentration that they could not be detected by secondary ion mass spectrometry or other typical compositional analysis techniques). Additionally, we remark that the structure of the emitters formed by the extrinsic defects could be complex—e.g., involving atoms and vacancies—and such that the point defects could annihilate and/or not be optically active at the boundary regions formed by dislocations or the surface. All these considerations are consistent with our observation that the emitters seem to form separately from the dislocations and away from the surface.

To summarize, we carried out a systematic study of a number of GaN samples with different characteristics tailored through different synthesis conditions. The goal was to study the effect of certain specific parameters—density of the dislocations, doping with foreign atoms, structure, and orientation of the grown GaN material—on the formation of single quantum emitters. We found no correlation between stacking faults and emitters; we found instead a rough—although not one-to-one—correlation between the number of emitters and the density of dislocations. However, the emitter locations and the dislocation sites are spatially distinct. Hence, we suggest that emitters relate to an as-yet-unidentified impurity or point defect in GaN whose density is affected by the extended defect density. Future engineering of single photon sources based on GaN will thus require engineering of both the impurity and extended defect density of these materials. Nevertheless the application of expensive bulk substrates, which tend to have low extended defect densities and a high density of unintentional n-dopants is likely to be unnecessary. Instead efforts to engineer these devices can focus on widely available GaN epitaxial layers on sapphire.

METHODS

Sample fabrication

Samples A and B consist of 2- and 4-μm thick undoped polar c-plane (0001) GaN grown on c-plane sapphire with different dislocation densities at 5×10^9 cm^{-2} (high dislocation density, HDD) and 3×10^8 cm^{-2} (low dislocation density, LDD), respectively. The HDD

Sample A was fabricated based on a 2D growth method, where a 30-nm GaN nucleation layer (NL) was grown at 540 °C and followed by the GaN growth at a V-III ratio of 1310. In the LDD Sample B, the NL was annealed at 1020 °C and followed by 3D growth using a low V-III ratio (715) and island coalescence was then enhanced by increasing the V-III ratio to 1075.[44] The dislocation reduction was achieved as the dislocations bend over and annihilate one another during the 3D-2D coalescence process.[45]

Sample C is c-plane GaN grown using an *ex situ*, prepatterned GaN/sapphire pseudosubstrate/seed layer (with a dislocation density of 5×10^9 cm^{-2}) with periodic SiO$_2$ stripes and an epitaxial lateral overgrowth technique. The GaN layer thickness is ~20 μm and the average dislocation density in the ELOG sample is 3×10^7 cm^{-2}. The ELOG process reduces the number of dislocations by physically stopping their propagation through the GaN film. The selected area epitaxy allows GaN to grow only where the underlying GaN seed layer is exposed (window region), whilst the GaN grows laterally over the mask (wing region), where dislocations would bend over during coalescence. The dislocation densities are measured to be 5×10^7 cm^{-2} and 9×10^6 cm^{-2} in the window and wing regions, respectively.

Sample D is a 2 μm carbon-doped GaN structure grown on graded AlGaN (1 μm) and/AlN (200 nm) buffer on a silicon (111) substrate. The dislocation density was estimated to be 2×10^9 cm^{-2}.

Sample E is 2-μm thick Fe-doped GaN (using Cp$_2$Fe as the precursor) grown on c-plane sapphire substrate with a dislocation density of 9×10^8 cm^{-2}.

Sample F is 2 μm n-doped GaN grown r-plane sapphire using silicon nitride interlayer and 3D-2D growth, which contains a typical dislocation density[46] of 4×10^9 cm^{-2}.

Sample G is 4 μm nonpolar (11-20) GaN grown using the 3D-2D method on m-plane sapphire with a dislocation density[38] of 3×10^{10} cm^{-2}.

Sample H is 4 μm semipolar (11-22) GaN grown on using 3D-2D method on m-plane sapphire with a dislocation density[38] of 3×10^{10} cm^{-2}.

Sample analysis

Optical characterization of the samples was performed in a lab-built confocal microscope using a 532-nm CW laser (Gem 532, Laser Quantum Ltd.) and a 710-nm CW laser (M2 SolsTiS Ti:Sapphire). Collection was done through a 0.9 NA air objective (TU Plan Fluor 100×, Nikon) and analyzed either through a spectrometer (SpectraPro Monochromator Acton SP2300, provided with a Pixis Camera 256, Princeton Instruments) or a pair of avalanche photodiodes (SPCM-AQR-14, Perkin Elmer) in a Hanbury-Brown and Twiss interferometer configuration. Samples were mounted on a XYZ positioning stage (P-611.3S, PI Nanocube). The AFM analysis was performed on a Dimension 3100 AFM in tapping mode. CL measurements were performed at room temperature in a Philips XL30s scanning electron microscope operating at 5 kV and equipped with a Gatan MonoCL4 system. TEM imaging was conducted in an Field Electron and Ion Company (FEI) Tecnai Osiris operated at 200 kV. The sample was prepared by standard mechanical polishing followed by Ar$^+$ ion milling at 5 kV and polishing at 1 kV down to 0.1 kV.

The multimicroscopy analysis combining CL, AFM, and PL measurements for the same area of the sample was done using a reference alignment grid patterned directly on the samples via electron beam lithography (EBL).

REFERENCES

[1] P. Müller, T. Tentrup, M. Bienert, G. Morigi, and J. Eschner, "Spectral properties of single photons from quantum emitters," Phys. Rev. A **96**(2), 023861 (2017).

[2] O. Gazzano, S. Michaelis de Vasconcellos, C. Arnold, A. Nowak, E. Galopin, I. Sagnes, L. Lanco, A. Lemaître, and P. Senellart, "Bright solid-state sources of indistinguishable single photons," Nat. Commun. **4**, 1425 (2013).

[3] N. Somaschi, V. Giesz, L. De Santis, J. C. Loredo, M. P. Almeida, G. Hornecker, S. L. Portalupi, T. Grange, C. Antón, J. Demory *et al.*, "Near-optimal single-photon sources in the solid state," Nat. Photonics **10**(5), 340–345 (2016).

[4] C. H. Bennett, G. Brassard, and N. D. Mermin, "Quantum cryptography without Bell's theorem," Phys. Rev. Lett. **68**, 557–559 (1992).

[5] K. R. Motes, J. P. Olson, E. J. Rabeaux, J. P. Dowling, S. J. Olson, and P. P. Rohde, "Linear optical quantum metrology with single photons: Exploiting spontaneously generated entanglement to Beat the shot-noise limit," Phys. Rev. Lett. **114**(17), 170802 (2015).

[6] S. Rajbhandari, J. J. D. McKendry, J. Herrnsdorf, H. Chun, G. Faulkner, H. Haas, I. M. Watson, D. O'Brien, and M. D. Dawson, "A review of gallium nitride LEDs for multi-gigabit-per-second visible light data communications," Semicond. Sci. Technol. **32**, 023001 (2017).

[7] I. Aharonovich, S. Castelletto, D. A. Simpson, C. H. Su, A. D. Greentree, and S. Prawer, "Diamond-based single-photon emitters," Rep. Prog. Phys. **74**(7), 076501 (2011).

[8] E. Neu, D. Steinmetz, J. Riedrich-Möller, S. Gsell, M. Fischer, M. Schreck, and C. Becher, "Single photon emission from silicon-vacancy colour centres in chemical vapour deposition nano-diamonds on iridium," New J. Phys. **13**(2), 025012 (2011).

[9] M. W. Doherty, N. B. Manson, P. Delaney, F. Jelezko, J. Wrachtrup, and L. C. L. Hollenberg, "The nitrogen-vacancy colour centre in diamond," Phys. Rep. **528**, 1–45 (2013).

[10] S. Castelletto, B. C. Johnson, C. Zachreson, D. Beke, I. Balogh, T. Ohshima, I. Aharonovich, and A. Gali, "Room temperature quantum emission from cubic silicon carbide nanoparticles," ACS Nano **8**(8), 7938–7947 (2014).

[11] Y. Zhou, Z. Wang, A. Rasmita, S. Kim, A. Berhane, Z. Bodrog, G. Adamo, A. Gali, I. Aharonovich, and W. B. Gao, "Room temperature solid-state quantum emitters in the telecom range," Sci. Adv. **4**(3), eaar3580 (2018).

[12] S. Choi, A. M. Berhane, A. Gentle, C. Ton-That, M. R. Phillips, and I. Aharonovich, "Electroluminescence from localized defects in zinc oxide: Toward electrically driven single photon sources at room temperature," ACS Appl. Mater. Interfaces **7**(10), 5619–5623 (2015).

[13] S. Choi, B. C. Johnson, S. Castelletto, C. Ton-That, M. R. Phillips, and I. Aharonovich, "Single photon emission from ZnO nanoparticles," Appl. Phys. Lett. **104**(26), 261101 (2014).

[14] T. T. Tran, K. Bray, M. J. Ford, M. Toth, and I. Aharonovich, "Quantum emission from hexagonal boron nitride monolayers," Nat. Nanotechnol. **11**(1), 37–41 (2016).

[15] T. T. Tran, C. Elbadawi, D. Totonjian, C. J. Lobo, G. Grosso, H. Moon, D. R. Englund, M. J. Ford, I. Aharonovich, and M. Toth, "Robust multicolor single photon emission from point defects in hexagonal boron nitride," ACS Nano **10**(8), 7331–7338 (2016).

[16]M. Arita, F. Le Roux, M. J. Holmes, S. Kako, and Y. Arakawa, "Ultraclean single photon emission from a GaN quantum dot," Nano Lett. **17**(5), 2902–2907 (2017).

[17]A. M. Berhane, K. Y. Jeong, Z. Bodrog, S. Fiedler, T. Schröder, N. V. Triviño, T. Palacios, A. Gali, M. Toth, D. Englund et al., "Bright room-temperature single-photon emission from defects in gallium nitride," Adv. Mater. **29**(12), 1605092 (2017).

[18]M. Palczewska, B. Suchanek, R. Dwilinski, K. Pakula, A. Wagner, and M. Kaminska, "Paramagnetic defects in GaN," MRS Internet J. Nitride Semicond. Res. **3**(45), e45 (1998).

[19]E. R. Glaser, W. E. Carlos, G. C. B. Braga, J. A. Freitas, W. J. Moore, B. V. Shanabrook, R. L. Henry, A. E. Wickenden, D. D. Koleske, H. Obloh et al., "Magnetic resonance studies of Mg-doped GaN epitaxial layers grown by organometallic chemical vapor deposition," Phys. Rev. B **65**(8), 085312 (2002).

[20]P. G. Baranov, I. V. Il'in, E. N. Mokhov, and V. A. Khramtsov, "Electron paramagnetic resonance of defects with metastable properties in crystalline GaN," Phys. Solid State **40**(10), 1648–1652 (1998).

[21]A. Denis, G. Goglio, and G. Demazeau, "Gallium nitride bulk crystal growth processes: A review," Mater. Sci. Eng., R **50**, 167–194 (2006).

[22]A. G. Curto, G. Volpe, T. H. Taminiau, M. P. Kreuzer, R. Quidant, and N. F. van Hulst, "Unidirectional emission of a quantum dot coupled to a nanoantenna," Science **329**(5994), 930–933 (2010).

[23]I. Aharonovich, D. Englund, and M. Toth, "Solid-state single-photon emitters," Nat. Photonics **10**, 631–641 (2016).

[24]L. Liu and J. H. Edgar, "Substrates for gallium nitride epitaxy," Mater. Sci. Eng., R **37**(3), 61–128 (2002).

[25]F. Scholz, "Semipolar GaN grown on foreign substrates: A review," Semicond. Sci. Technol. **27**(2), 024002 (2012).

[26]Y. S. Lee, T. H. Seo, A. H. Park, K. J. Lee, S. J. Chung, and E. K. Suh, "Influence of controlled growth rate on tilt mosaic microstructures of nonpolar a-plane GaN epilayers grown on R-plane sapphire," Electron. Mater. Lett. **8**(3), 335–339 (2012).

[27]W. Wang, W. Yang, H. Wang, Y. Zhu, M. Yang, J. Gao, and G. Li, "A comparative study on the properties of c-plane and a-plane GaN epitaxial films grown on sapphire substrates by pulsed laser deposition," Vacuum **128**, 158–165 (2016).

[28]Z. Liliental-Weber, "GaN grown in polar and non-polar directions," Opto-Electron. Rev. **12**(4), 339–346 (2004).

[29]P. Kozodoy, H. Xing, S. P. DenBaars, U. K. Mishra, A. Saxler, R. Perrin, S. Elhamri, and W. C. Mitchel, "Heavy doping effects in Mg-doped GaN," J. Appl. Phys. **87**(4), 1832–1835 (2000).

[30]S. Heikman, S. Keller, T. Mates, S. P. DenBaars, and U. K. Mishra, "Growth and characteristics of Fe-doped GaN," J. Cryst. Growth **248**, 513–517 (2003).

[31]S. Tomiya, T. Hino, S. Goto, M. Takeya, and M. Ikeda, "Dislocation related issues in the degradation of GaN-based laser diodes," IEEE J. Sel. Top. Quantum Electron. **10**(6), 1277–1286 (2004).

[32]A. M. Jeffries, L. Ding, J. J. Williams, T. L. Williamson, M. A. Hoffbauer, C. B. Honsberg, and M. I. Bertoni, "Gallium nitride grown by molecular beam epitaxy at low temperatures," Thin Solid Films **642**, 25–30 (2017).

[33]H. Masui, S. Nakamura, S. P. DenBaars, and U. K. Mishra, "Nonpolar and semipolar III-nitride light-emitting diodes: Achievements and challenges," IEEE Trans. Electron Devices **57**(1), 88–100 (2010).

[34]G. Li, W. Wang, W. Yang, Y. Lin, H. Wang, Z. Lin, and S. Zhou, "GaN-based light-emitting diodes on various substrates: A critical review," Rep. Prog. Phys. **79**, 056501 (2016).

[35]H. P. Xin and C. W. Tu, "GaInNAs/GaAs multiple quantum wells grown by gas-source molecular beam epitaxy," Appl. Phys. Lett. **72**(19), 2442–2444 (1998).

[36]F. C. P. Massabuau, S. L. Sahonta, L. Trinh-Xuan, S. Rhode, T. J. Puchtler, M. J. Kappers, C. J. Humphreys, and R. A. Oliver, "Morphological, structural, and emission characterization of trench defects in InGaN/GaN quantum well structures," Appl. Phys. Lett. **101**(21), 212107 (2012).

[37]C. F. Johnston, M. A. Moram, M. J. Kappers, and C. J. Humphreys, "Defect reduction in (112̄2) semipolar GaN grown on M-plane sapphire using ScN interlayers," Appl. Phys. Lett. **94**(16), 161109 (2009).

[38]F. Oehler, D. Sutherland, T. Zhu, R. Emery, T. J. Badcock, M. J. Kappers, C. J. Humphreys, P. Dawson, and R. A. Oliver, "Evaluation of growth methods for the heteroepitaxy of non-polar (1120) GaN on sapphire by MOVPE," J. Cryst. Growth **408**, 32–41 (2014).

[39]T. Zhu and R. A. Oliver, "Unintentional doping in GaN," Phys. Chem. Chem. Phys. **14**, 9558–9573 (2012).

[40]M. Nguyen, S. Kim, T. T. Tran, Z. Q. Xu, M. Kianinia, M. Toth, and I. Aharonovich, "Nanoassembly of quantum emitters in hexagonal boron nitride and gold nanospheres," Nanoscale **10**(5), 2267–2274 (2018).

[41]C. Jardin, B. Canut, and S. M. M. Ramos, "The luminescence of sapphire subjected to the irradiation of energetic hydrogen and helium ions," J. Phys. D: Appl. Phys. **29**(8), 2066–2070 (1996).

[42]S. K. Rhode, M. K. Horton, M. J. Kappers, S. Zhang, C. J. Humphreys, R. O. Dusane, S. L. Sahonta, and M. A. Moram, "Mg doping affects dislocation core structures in GaN," Phys. Rev. Lett. **111**(2), 025502 (2013).

[43]N. Yamamoto, H. Itoh, V. Grillo, S. F. Chichibu, S. Keller, J. S. Speck, S. P. DenBaars, U. K. Mishra, S. Nakamura, and G. Salviati, "Cathodoluminescence characterization of dislocations in gallium nitride using a transmission electron microscope," J. Appl. Phys. **94**(7), 4315–4319 (2003).

[44]S. Kim, J. Oh, J. Kang, D. Kim, J. Won, J. Kim, and H. Cho, "Two-step growth of high quality GaN using V/III ratio variation in the initial growth stage," J. Cryst. Growth **262**(1-4), 7–13 (2004).

[45]A. Y. Polyakov, L. W. Jang, N. B. Smirnov, A. V. Govorkov, E. A. Kozhukhova, T. G. Yugova, V. Y. Reznik, S. J. Pearton, K. H. Baik, S. M. Hwang et al., "Characteristics of a-GaN films and a-AlGaN/GaN heterojunctions prepared on R-sapphire by two-stage growth process," J. Appl. Phys. **110**(9), 093709 (2011).

[46]T. Zhu, D. Sutherland, T. J. Badcock, R. Hao, M. A. Moram, P. Dawson, M. J. Kappers, and R. A. Oliver, "Defect reduction in semi-polar (11-22) gallium nitride grown using epitaxial lateral overgrowth," Jpn. J. Appl. Phys., Part 2 **52**(8), 08JB01 (2013).